Augmented Unscented Kalman Filter-Based Method for Voltage Sag Detection and Characterization

Doan Duc Tung, Ngo Minh Khoa*

Faculty of Engineering and Technology, Quy Nhon University, Quy Nhon Nam, Vietnam

ABSTRACT: This paper proposes an Augmented Unscented Kalman Filter (AUKF)-based approach for the detection and characterization of voltage sag events in power systems. Unlike the Extended Kalman Filter (EKF), which requires Jacobian computation, and the conventional Unscented Kalman Filter (UKF), which may suffer from reduced numerical stability, the proposed AUKF formulation incorporates augmented state variables to accurately estimate distorted waveforms including harmonics with improved computational efficiency. The proposed method is validated through numerical simulations of voltage sag events with different residual magnitudes (0.2, 0.5, and 0.8 p.u.). Comparative analysis shows that the AUKF achieves lower root-mean-square error (RMSE ≈ 0.015 p.u.) and higher detection accuracy (>97%) compared with the UKF (RMSE ≈ 0.021 p.u., accuracy ≈ 96%) and the EKF (RMSE ≈ 0.028 p.u., accuracy ≈ 95%). These results demonstrate that the AUKF-based algorithm not only enhances accuracy and robustness in voltage sag detection but also ensures computational efficiency, making it suitable for real-time power quality monitoring applications.

KEYWORDS: Augmented Unscented Kalman filter, Power quality, Signal processing, Voltage harmonics, Voltage sag detection.

[Received Jan. 01, 2025; Revised Jul. 24, 2025; Accepted Oct. 12, 2025] Print ISSN: 0189-9546 | Online ISSN: 2437-2110

I. INTRODUCTION

Voltage variations, particularly voltage sags and interruptions, are among the most critical power quality (PQ) disturbances in distribution networks. Although customers generally recognize that such disturbances cannot be entirely eliminated in distribution systems (Bollen 2000), their tolerance decreases significantly when voltage sags cause equipment malfunctions, since these events occur much more frequently than complete interruptions. Voltage sags are characterized by transient reductions in the root-mean-square (RMS) voltage magnitude supplied to end-users. The severity of their impact is determined by several factors, including the magnitude of the voltage drop, the event duration, and the sensitivity of the affected equipment (Bollen and Gu, 2006). Effective detection and characterization of these disturbances are, therefore, essential for mitigating their adverse effects on power systems and end-user equipment.

Analyzing voltage sags has become increasingly valuable for utilities when assessing PQ levels at newly constructed industrial and commercial sites. By predicting the expected PQ levels in advance, utilities enable their customers to proactively implement solutions for mitigating voltage sags during the facility's design and construction phases. Moreover, this analysis allows utilities to evaluate the impacts of network modifications on customer PQ levels. For instance, integrating additional generation resources can reduce the frequency and severity of voltage sags, while reconfiguring tie switches or adding transmission lines may also influence overall network performance. A voltage sag is typically described as a temporary drop in RMS voltage magnitude lasting for a specified time period. Among PQ disturbances, voltage sag is both the most significant and the most frequently encountered. Definitions for voltage sag vary across standards, particularly regarding duration and magnitude. According to IEEE Standard 1159-1995, a voltage sag is specified as a reduction in the RMS voltage in the range of 0.1 and 0.9 per unit, lasting from 0.5 cycles to 1 minute. The sag event starts when the Urms (1/2) voltage drops below the defined limit and stops when the Urms (1/2) voltage recovers to a value equal to or exceeding the sag limit plus the hysteresis voltage. The residual voltage represents the minimum Urms (1/2) voltage observed during the sag, while the sag duration is calculated as the time difference between the event's initiation and conclusion. Voltage sags may arise from various sources, including short circuit, transformer energization, and starting heavy loads. Numerous signal processing and statistical analysis methods have been explored for detecting and classifying PQ disturbances (Mansor and Rahim, 2009), (Chang and Chen, 2010), (Granados-Lieberman *et al,* 2011), (Pérez and Barros, 2006), (Perez and Barros, 2008). Among these, wavelet transform (WT) has emerged as a key signal processing technique for analyzing PQ events, with extensive research detailing its application for detecting and classifying power quality disturbances (Costa *et al*, 2010), (Yu *et al,* 2021), (Gencer *et al*, 2010), (Masoum *et al,* 2010). Additionally, advanced techniques such as the S-transform and

*Corresponding author: *ngominhkhoa@qnu.edu.vn*

doi: http://doi.org/10.63746/njtd.v22i5.3247

neural networks were successfully applied to identify PQ disturbances (Ai *et al*, 2007), (Mishra *et al*, 2007). For handling nonlinear systems, two advanced filtering approaches, the extended Kalman filter (EKF) and unscented Kalman filter (UKF) were proposed. The EKF requires the computation of Jacobian matrices, whereas the UKF leverages the unscented transform as a deterministic sampling technique, thereby offering improved computational efficiency (Perez and Barros, 2008), (Hartikainen *et al*, 2011).

Recent studies have increasingly focused on hybrid and machine-learning-based approaches for PQ event detection. For example, (Choudhury *et al*, 2024) employed ensemble extreme learning machines for PV-integrated systems, while (Tong *et al*, 2023) and (Wang *et al*, 2025) explored adaptive decomposition and neural network-based models for sag classification. Although these approaches achieve high classification accuracy, they often require extensive training data and involve heavy computational loads. By contrast, the proposed AUKF-based method provides a model-driven solution with lower computational complexity, while still ensuring high detection accuracy and robustness under noise. This distinction highlights the novelty of our contribution, as the proposed AUKF framework combines computational efficiency with robustness to harmonics, which has not been fully achieved in recent works.

Previous studies using the EKF (Perez and Barros, 2008) have suffered from the need to compute Jacobians, which often leads to causes divergence under nonlinear conditions. UKF approaches partially addressed this limitation, but their accuracy decreases in the presence of harmonic distortion, and computational costs remain significant. Wavelet-based methods, while effective in capturing transient features, are sensitive to parameter selection and computationally heavy for online applications. To address these gaps, this paper introduces an AUKF-based algorithm that incorporates augmented states to capture both fundamental and harmonic components, avoids Jacobian computations, and achieves robust and efficient sag detection suitable for real-time implementation. This paper proposes a new algorithm for voltage sag detection by applying the AUKF. The main contributions of this paper can be summarized as follows:

- An AUKF-based framework is proposed for voltage sag detection and characterization, which avoids Jacobian computation in EKF and improves numerical stability compared with conventional UKF.
- Through simulation studies the proposed method demonstrated significant improvements in accuracy and efficiency compared with EKF and UKF approaches.
- The proposed method enables not only sag detection but also precise estimation of residual magnitude and event duration, making it suitable for real-time power quality monitoring.

II. VOLTAGE SAG CHARACTERIZATION

A. Definition of Voltage Sag

In accordance with the power quality standard IEC 1159-2009, a voltage sag is specified as an event where the RMS voltage magnitude decreases to a range between 10% and 90% of the nominal value, persisting for a duration from 0.5 cycles to 1 minute. The main characteristic parameters of a voltage sag event are illustrated in Figure 1. The main parameters of a voltage sag are described as follows:

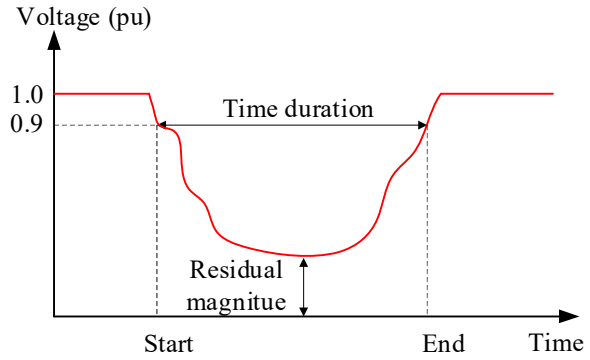

Figure 1 The voltage sag characteristics.

B. The Residual Magnitude

A residual magnitude is one of the most important indicators for assessing the severity of a voltage sag event. The residual magnitude varies with its underlying cause. In short-circuit events, the sag magnitude is determined at the Point of Common Coupling (PCC). This determination is based on a simplified system model, as depicted in Figure 2. The PCC serves as the reference point where the system impedance and the fault location collectively influence the severity of the voltage sag observed by end-users.

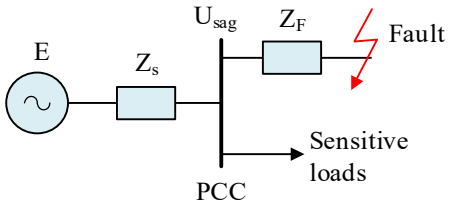

Figure 2 Simple model for calculating voltage sag.

The PCC's voltage is determined as follows:

$$U_{sag} = \frac{Z_F}{Z_s + Z_F} E \quad (1)$$

Assuming that $E = 1$ (pu), then the voltage sag magnitude will be:

$$U_{sag} = \frac{Z_F}{Z_s + Z_F} \quad (2)$$

where Z_F is the fault impedance calculated by $Z_F = zL$, where z represents the total line impedance and L represents the distance from the PCC to the fault location, Eq. (2) can be reformulated as follows: (2) can be reformulated as follows:

$$U_{sag} = \frac{zL}{Z_s + zL} \quad (3)$$

Equation (3) indicates that the voltage sag becomes deeper when short-circuit faults occur close to the customer and when the short-circuit power capacity is small (i.e., the total impedance is large). Consider the 22-kV distribution network model illustrated in Figure 2. In which the power supply has short-circuit power levels of 750, 200, and 75 MVA, the inner resistance of the power supply is assumed to be ignored. The

120-mm^2 cross-section overhead line has an impedance of $z = 0.117 + j0.315$ (Ω/km). The impact of the short-circuit power on the voltage mgnitude is shown as Figure 3.

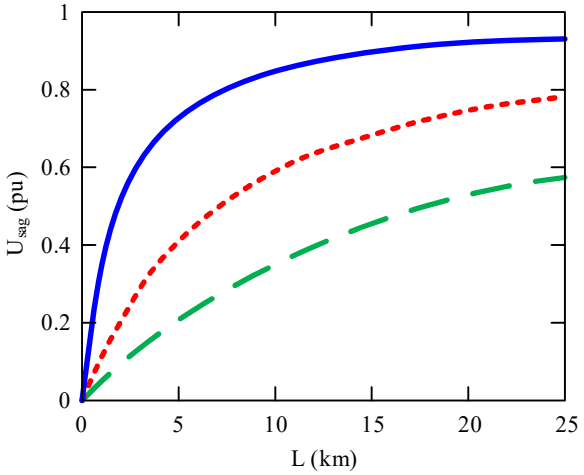

Figure 3 Impact of short-circuit power on voltage sag magnitude.

We re-consider the aforementioned distribution network model but it is assumed that the power supply has a short-circuit power capacity of 200 MVA; the overhead line has different cross sections of 50, 120 and 240 mm^2 with unit impedances of $z = 0.363 + j0.351$ (Ω/km); $z = 0.117 + j0.351$ (Ω/km); and $z = 0.061 + j0.298$ (Ω/km). The simulation results of voltage sag magnitude depending on the conductor cross section are shown in Figure 4.

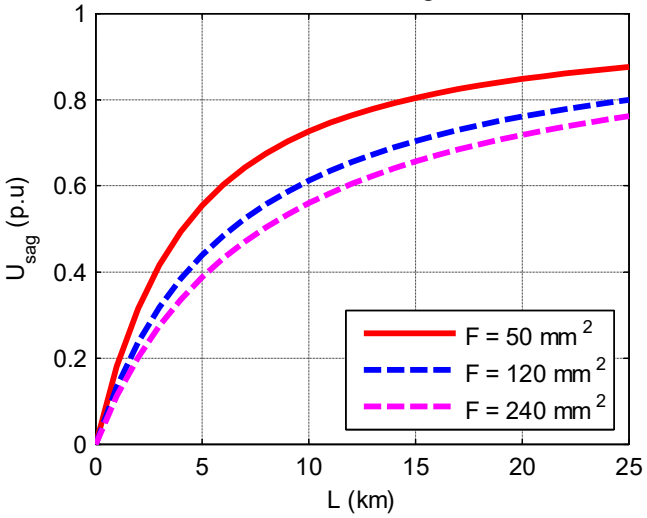

Figure 4 The impact of conductor cross-section on residual magnitude.

C. Time Duration

The time duration of a voltage sag event depends on its underlying cause. For voltage sags due to short circuit in the power system, the time duration of the event shall be determined by the duration of the action of the protection relay. In transmission networks, the main protection devices typically have a fault clearing time of about 60–150 ms. In distribution networks, the main protection devices, such as circuit breakers and fuses, are overcurrent relays with either independent or dependent time characteristics. The fault clearing time of protection relays typically ranges between 0.5 and 2 seconds. This duration depends on the relay settings, system configuration, and the nature of the fault, and it significantly influences the overall impact of voltage sags on the power system and connected equipment.

D. Phase-Angle Jump

A phase-angle jump refers to the instantaneous shift in the voltage phase at the onset of a voltage sag event (Bollen and Gu, 2006). Figure 2 is also employed to determine the phase angle jump of the voltage sag. Let $Z_S = R_S + jX_S$; $Z_F = R_F + jX_F$, where Z_S, Z_F represent the source impedance and fault impedance, respectively. Given the change in the voltage phase angle during the sag, the argument of U_{sag} can be determined as follows:

$$\Delta\phi = \arg(U_{sag}) = \arctan\left(\frac{X_F}{R_F}\right) - \arctan\left(\frac{X_F + X_S}{R_F + R_S}\right) \quad (4)$$

If $\frac{X_F}{R_F} = \frac{X_S}{R_S}$ then Eq. (4) will be zero, indicating that there is no phase angle jump for the voltage sag. Therefore, a phase-angle jump only occurs when the ratio of source impedance to line impedance differs. For voltage sags caused by short-circuit faults, the phase angle jump is influenced by various network parameters that come into play once the fault event begins. These parameters include the short-circuit ratio X_N/R_N and the phase-angle shift caused by changes in the wiring configuration between the primary and secondary sides of the transformer (Choudhury *et al*, 2024).

III. METHODOLOGY BACKGROUND

A. The Matrix Formulation of Unscented Transform

The unscented transform (Bollen and Gu, 2006) can be expressed in a matrix formulation as follows:

$$\mathbf{X} = [\mathbf{m} \quad \dots \quad \mathbf{m}] + [\mathbf{0} \quad \sqrt{\mathbf{P}} \quad -\sqrt{\mathbf{P}}] \times \sqrt{\mathbf{c}} \quad (5)$$

$$\mathbf{Y} = \mathbf{g}(\mathbf{X}) \quad (6)$$

$$\boldsymbol{\mu}_U = \mathbf{Y}\mathbf{w}_m \quad (7)$$

$$\mathbf{S}_U = \mathbf{Y}\mathbf{W}\mathbf{Y}^T \quad (8)$$

$$\mathbf{C}_U = \mathbf{X}\mathbf{W}\mathbf{Y}^T \quad (9)$$

where T denotes the transposition matrix, $\mathbf{X}$ is the sigma point matrix, and the function $\mathbf{g}(\cdot)$ is applied to each column of the argument matrix independently. The constant $\mathbf{c} = (n + k) \times \alpha^2$, where α, n, and k are specific parameters. Additionally, the weight vector $\mathbf{w}_m$ and the matrix $\mathbf{W}$ are expressed as follows:

$$\mathbf{w}_m = \left[\mathbf{W}_m^{(0)} \quad \dots \quad \mathbf{W}_m^{(2n)}\right]^T \quad (10)$$

$$\mathbf{W} = (\mathbf{I} - [\mathbf{w}_m \quad \dots \quad \mathbf{w}_m]) \times \mathbf{diag}\left(\mathbf{W}_c^{(0)} \quad \dots \quad \mathbf{W}_c^{(2n)}\right) \quad (11)$$

The filtering model utilized in the AUKF is formulated as follows:

$$\mathbf{x}_k = \mathbf{f}(\mathbf{x}_{k-1}, k-1) + \mathbf{q}_{k-1}$$
$$\mathbf{y}_k = \mathbf{h}(\mathbf{x}_k, k) + \mathbf{r}_k \quad (12)$$

where $\mathbf{x}_k \in \Re^n$ represents the state vector, $\mathbf{y}_k \in \Re^m$ is the measurement vector, $\mathbf{q}_{k-1} \sim N(\mathbf{0}, \mathbf{Q}_{k-1})$ is the Gaussian process noise with the zero mean and covariance, and $\mathbf{r}_k \sim N(\mathbf{0}, \mathbf{R}_k)$ is the Gaussian measurement noise with the zero mean and covariance. The function $\mathbf{f}(\cdot)$ denotes the non-linear

dynamic model, while $\mathbf{h}(\cdot)$ represents the non-linear measurement function.

The AUKF (Bollen and Gu, 2006), (Perez and Barros, 2008), (Hartikainen *et al*, 2011) is divided into two steps:

+ *Prediction:* To predict the state, first form the sigma point matrix for the augmented state variables $\tilde{\mathbf{x}}_{k-1} = [\mathbf{x}_{k-1}^T \quad \mathbf{q}_{k-1}^T \quad \mathbf{r}_{k-1}^T]^T$ as follows:

$$\tilde{\mathbf{X}}_{k-1} = [\tilde{\mathbf{m}}_{k-1} \quad \dots \quad \tilde{\mathbf{m}}_{k-1}] + \sqrt{\mathbf{c}}\left[\mathbf{0} \quad \sqrt{\tilde{\mathbf{P}}_{k-1}} \quad -\sqrt{\tilde{\mathbf{P}}_{k-1}}\right] \tag{13}$$

where

$$\tilde{\mathbf{m}}_{k-1} = [\mathbf{m}_{k-1}^T \quad \mathbf{0} \quad \mathbf{0}] \tag{14}$$

And

$$\tilde{\mathbf{P}}_{k-1} = \begin{bmatrix} \mathbf{P}_{k-1} & \mathbf{0} & \mathbf{0} \\ \mathbf{0} & \mathbf{Q}_{k-1} & \mathbf{0} \\ \mathbf{0} & \mathbf{0} & \mathbf{R}_{k-1} \end{bmatrix} \tag{15}$$

Next, the predicted state mean $\mathbf{m}_k^-$ and covariance $\mathbf{P}_k^-$ are calculated as follows:

$$\begin{aligned} \hat{\mathbf{X}}_k &= \mathbf{f}\left(\mathbf{X}_{k-1}^x, \mathbf{X}_{k-1}^q, k-1\right) \\ \mathbf{m}_k^- &= \hat{\mathbf{X}}_k \mathbf{w}_m \\ \mathbf{P}_k^- &= \hat{\mathbf{X}}_k \mathbf{W} \left[\hat{\mathbf{X}}_k\right]^T \end{aligned} \tag{16}$$

+ *Update:* Compute the predicted mean $\boldsymbol{\mu}_k$ and measurement covariance $\mathbf{S}_k$, as well as the state and measurement cross-covariance $\mathbf{C}_k$, as follows:

$$\begin{aligned} \mathbf{Y}_k^- &= \mathbf{h}\left(\hat{\mathbf{X}}_k, \mathbf{X}_{k-1}^r, k\right) \\ \boldsymbol{\mu}_k &= \mathbf{Y}_k^- \mathbf{w}_m \\ \mathbf{S}_k &= \mathbf{Y}_k^- \mathbf{W} [\mathbf{Y}_k^-]^T \\ \mathbf{C}_k &= \hat{\mathbf{X}}_k \mathbf{W} [\mathbf{Y}_k^-]^T \end{aligned} \tag{17}$$

Subsequently, the filter gain $\mathbf{K}_k$, the updated state mean $\mathbf{m}_k$ and covariance $\mathbf{P}_k$ are calculated as follows:

$$\begin{aligned} \mathbf{K}_k &= \mathbf{C}_k \mathbf{S}_k^{-1} \\ \mathbf{m}_k &= \mathbf{m}_k^- + \mathbf{K}_k [\mathbf{y}_k - \boldsymbol{\mu}_k] \\ \mathbf{P}_k &= \mathbf{P}_k^- - \mathbf{K}_k \mathbf{S}_k \mathbf{K}_k^T \end{aligned} \tag{18}$$

B. Signal Model

The power system voltage waveform is assumed to consist of both fundamental and harmonic components (Camarillo-Peñaranda and Ramos, 2018), (Li *et al*, 2022), (Stuart *et al*, 2021) and can be expressed as follows:

$$y(t) = \sum_{i=1}^{N} a_i(t) \sin\left(i\omega(t)t + \varphi_i(t)\right) \tag{19}$$

where $a_i(t)$ and $\varphi_i(t)$ represent the magnitude and phase of the i^{th} harmonic component, respectively. N denotes the total harmonic order number, and $\omega(t)$ is the angular frequency of the fundamental component of the signal under disturbance. In this study, the total harmonic order N was fixed to 7 for simulation purposes, which covers the most significant harmonic orders observed in distribution systems. However, the model formulation supports arbitrary values of N depending on the application.

In this scenario, the system nonlinearity is established via the measurement model. However, it is also able to represent the nonlinearity within the dynamic model, thereby allowing the measurement model to remain linear (Hasan *et al*, 2020), (Han *et al*, 2019), (Wang *et al*, 2022). In this case, the state vector can be rewritten as follows:

$$\mathbf{x}_k = (\theta_k \quad \omega_k \quad a_{1k} \quad \dots \quad a_{Nk} \quad \varphi_{1k} \quad \dots \quad \varphi_{Nk})^T \tag{20}$$

where θ_k is the phase angle at the time step k, ω_k is the angular velocity at the time step k, a_{ik} and φ_{ik} represent the magnitude and phase angle of the i^{th} component at the time step k, respectively. The evolution parameter θ_k is modeled using a discretized Wiener velocity model, in which the velocity corresponds to the angular velocity:

$$\frac{d\theta}{dt} = \omega \tag{21}$$

ω, a_i and φ_i are perturbed by one-dimensional white noise processes $w_\omega(t)$, $w_{ai}(t)$ and $w_{\varphi i}(t)$, respectively. As a result, the signal is no longer entirely deterministic:

$$\begin{aligned} \frac{d\omega}{dt} &= w_\omega(t) \\ \frac{da_i}{dt} &= w_{ai}(t), i = 1,3, \dots N \\ \frac{d\varphi_i}{dt} &= w_{\varphi i}(t), i = 1,3, \dots N \end{aligned} \tag{22}$$

The continuous-time dynamic equation can be expressed as follows:

$$\frac{d\mathbf{x}(t)}{dt} = \mathbf{F}\mathbf{x}(t) + \mathbf{L}\mathbf{w}(t) \tag{23}$$

where $\mathbf{F}$ is a matrix with the dimension of $(2N + 2 \times 2N + 2)$, and $\mathbf{L}$ is a matrix $(2N + 2 \times 2N + 1)$, as shown below:

$$\mathbf{F} = \begin{pmatrix} 0 & 1 & 0 & \dots & 0 \\ 0 & 0 & 0 & \dots & 0 \\ 0 & 0 & 0 & \dots & 0 \\ \vdots & \vdots & \vdots & \ddots & \vdots \\ 0 & 0 & 0 & \dots & 0 \end{pmatrix} \tag{24}$$

$$\mathbf{L} = \begin{pmatrix} 0 & 0 & \dots & 0 \\ 1 & 0 & \dots & 0 \\ 0 & 1 & \dots & 0 \\ \vdots & \vdots & \ddots & \vdots \\ 0 & 0 & \dots & 1 \end{pmatrix} \tag{25}$$

And

$$\mathbf{w}(t) = \begin{pmatrix} w_\omega(t) \\ w_{a1}(t) \\ \vdots \\ w_{aN}(t) \\ w_{\varphi 1}(t) \\ \vdots \\ w_{\varphi N}(t) \end{pmatrix} \tag{26}$$

The continuous-time model Eqs. (23)–(26) is discretized using a zero-order hold with step size $\Delta t = 156\ \mu s$ (corresponding to a sampling rate of 6.4 kHz). This choice ensures numerical stability while preserving waveform fidelity. Therefore, the discretized dynamic equation can be expressed as follows:

$$\mathbf{x}_k = \mathbf{A}\mathbf{x}_{k-1} + \mathbf{q}_{k-1} \tag{27}$$

where Δt is the step size and $\mathbf{A}$ is a matrix with the dimension of $(2N + 2 \times 2N + 2)$

$$\mathbf{A} = \begin{pmatrix} 1 & \Delta t & 0 & \dots & 0 \\ 0 & 1 & 0 & \dots & 0 \\ 0 & 0 & 1 & \dots & 0 \\ \vdots & \vdots & \vdots & \ddots & \vdots \\ 0 & 0 & 0 & \dots & 1 \end{pmatrix} \tag{28}$$

In this case, the nonlinearity is expressed through the measurement model. Specifically, the current state is

propagated through a nonlinear measurement function $\mathbf{h}(\mathbf{x}_k, k)$ to obtain the actual measurement. The function is the sine function.

$$\mathbf{h}(\mathbf{x}_k, k) = \sum_{i=1}^{N} a_{ik} \sin(i\theta_k + \varphi_{ik}) \quad (29)$$

With this, the measurement model can be expressed as follows:

$$\mathbf{y}_k = \mathbf{h}(\mathbf{x}_k, k) + \mathbf{r}_k = \sum_{i=1}^{N} a_{ik} \sin(i\theta_k + \varphi_{ik}) + \mathbf{r}_k \quad (30)$$

C. Detection and Characterization Algorithm for Voltage Sag

This paper proposes an algorithm for detecting and characterizing of voltage sag events utilizing the Augmented Unscented Kalman Filter (AUKF). First, the voltage sag waveforms are modeled in Section B. Then, the AUKF is applied to estimate the signals. The error (e_k) between the real and estimated signal which is identified by (28) is applied to detect the beginning and end of voltage sag.

$$e_k = \hat{y}_k - y_k \quad (31)$$

where y_k denotes the real signal and $\hat{y}_k$ represents the estimated signal.

Voltage magnitude which is estimated by AUKF during event is used to calculate the magnitude signal. The sag detection is triggered when $|e(k)|$ exceeds a predefined threshold $T = 0.05$ p.u., or equivalently when the error surpasses three times the noise standard deviation (3σ criterion). This ensures robustness against false alarms due to measurement noise.

Voltage magnitude which is estimated by AUKF during event is used to calculate the magnitude signal. The sag detection is triggered when $|e(k)|$ exceeds a predefined threshold $T = 0.05$ p.u., or equivalently when the error surpasses three times the noise standard deviation (3σ criterion). This ensures robustness against false alarms due to measurement noise. Fig. 5 illustrates the flowchart of the proposed algorithm for voltage sag detection and characterization based on the Augmented Unscented Kalman Filter (AUKF). The process begins with the acquisition of the input voltage signal. The AUKF is then applied to estimate the instantaneous voltage waveform, producing a reconstructed signal that accounts for system nonlinearities. The difference between the measured and estimated signals is computed and continuously monitored. When this error exceeds a predefined threshold determined by the three-sigma criterion the algorithm identifies the onset of a sag event. Similarly, the event is marked as completed once the error returns below the threshold. In parallel, the estimated magnitude signal is used to calculate the residual voltage, while the timestamps of detection allow accurate estimation of sag duration. The integration of these steps ensures that both the temporal and magnitude characteristics of the sag are reliably captured. Overall, the flowchart highlights the sequential operations of the AUKF-based framework, emphasizing its ability to detect, localize, and characterize voltage sags in real time with high robustness against noise.

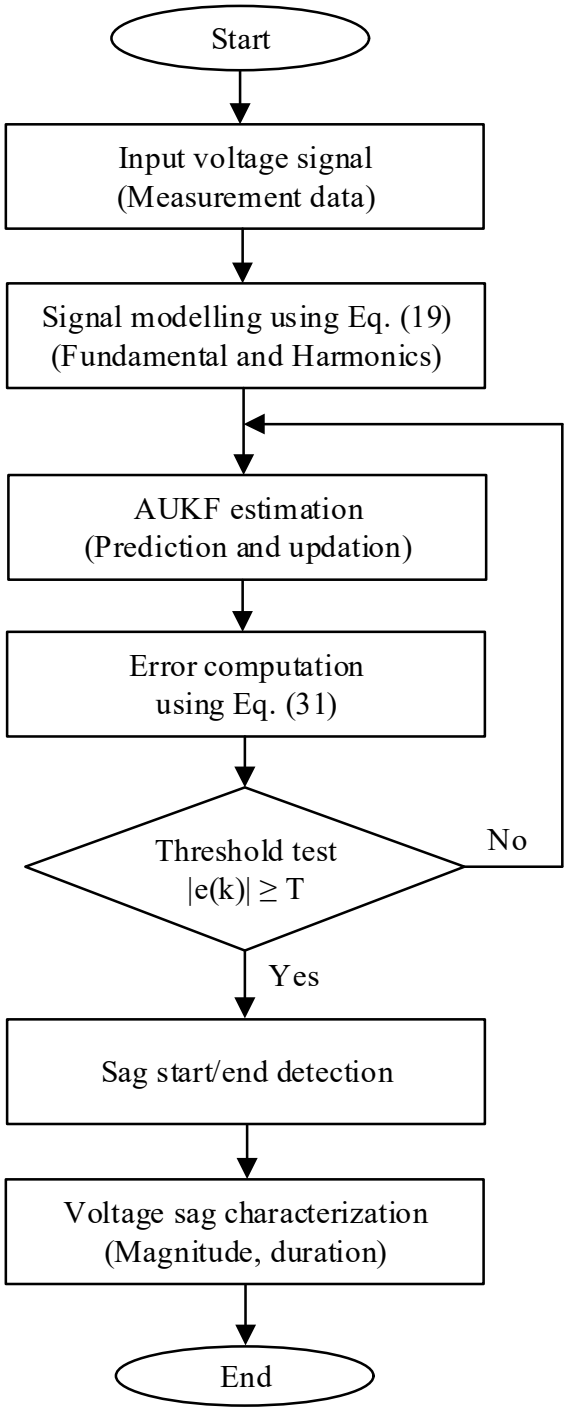

Figure 5 The algorithm for voltage sag detection and characterization using the AUKF.

IV. VOLTAGE SAG DETECTION AND CHARACTERIZATION

To assess the suitability of the proposed algorithm for voltage sag detection, we compare it with existing methods. In this section, voltage sag waveforms with residual magnitudes of 0.2, 0.5, and 0.8 p.u. were considered. Additionally, the mathematical model for voltage sag is assumed to be represented by the following equations. The voltage signal, as

described by the voltage sag waveform, is modelled by the following equation:

$$u(t) = U_m \sin(2\pi ft + \varphi) \quad (32)$$

where U_m is the voltage magnitude; f is the frequency; t is the time and φ is the phase angle. The voltage sag waveform is established by using Eq. (32) in MATLAB with the sampling frequency of 6.4 kHz.

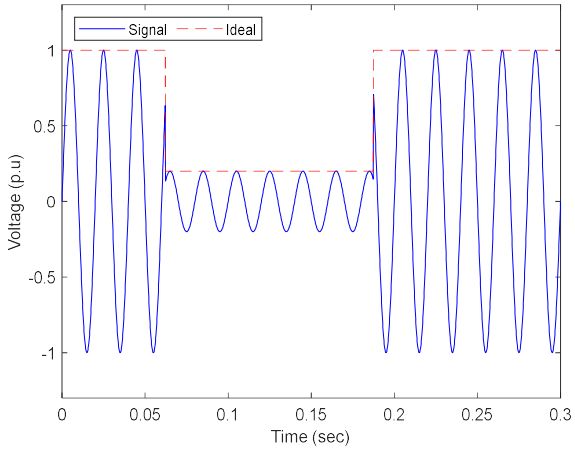

(a) Voltage waveform

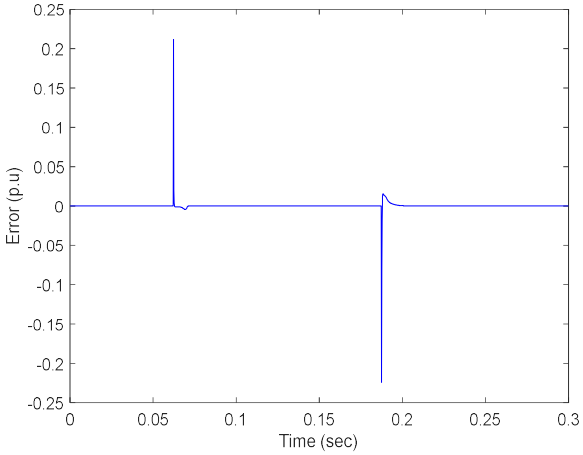

(b) Error of AUKF

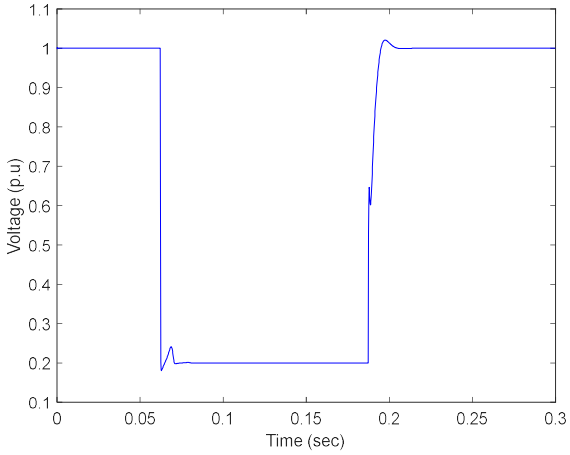

(c) Magnitude estimation

Figure 6 Estimation results of voltage sag with residual magnitude of 0.2 p.u.

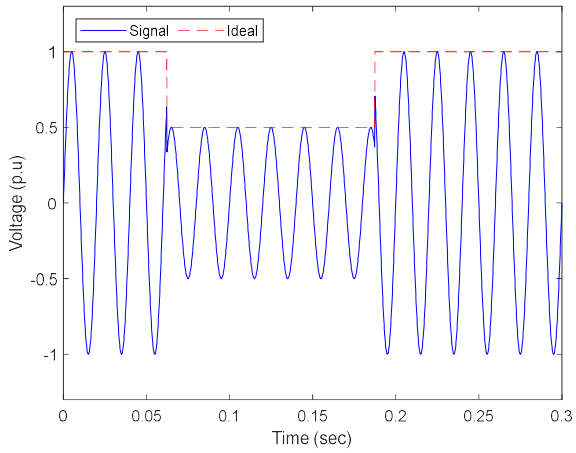

(a) Voltage waveform

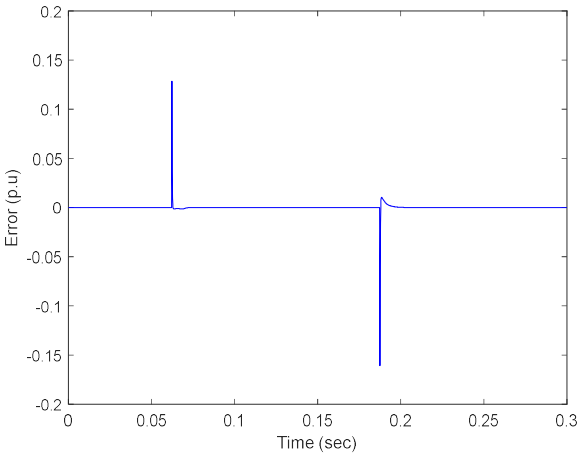

(b) Error of AUKF

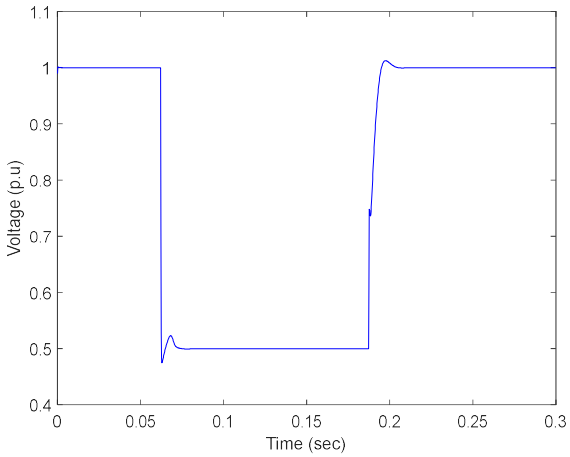

(c) Magnitude estimation

Figure 7 Estimation results of voltage sag with residual magnitude of 0.5 p.u.

The parameter estimation results for voltage sags with residual magnitudes of 0.2, 0.5, and 0.8 p.u. are presented in Figure 6, Figure 7, and Figure 8, respectively. For these three cases, the starting time of the voltage sag is 0.0625 sec and the ending time is 0.1875 sec. The magnitude of the ideal voltage signal is shown on the same graph of the voltage sag waveform

in Figure 6a (For voltage sag with the magnitude of 0.2 p.u), Figure 7a (For voltage sag with the magnitude of 0.5 p.u) and Figure 8a (For voltage sag with the magnitude of 0.8 p.u). This ideal characteristic of the voltage sag magnitude is considered as the reference value to evaluate the estimation ability of the AUKF method in this study.

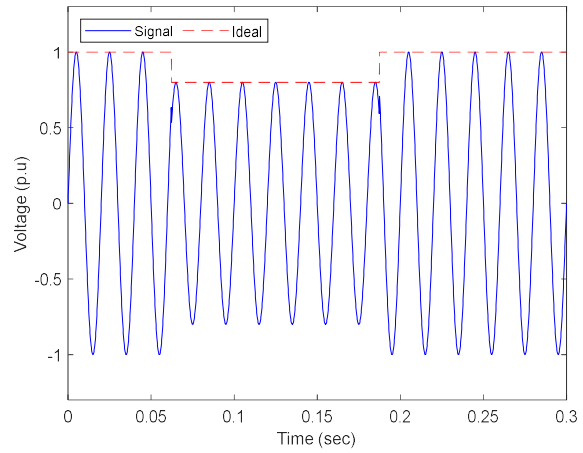

(a) Voltage waveform

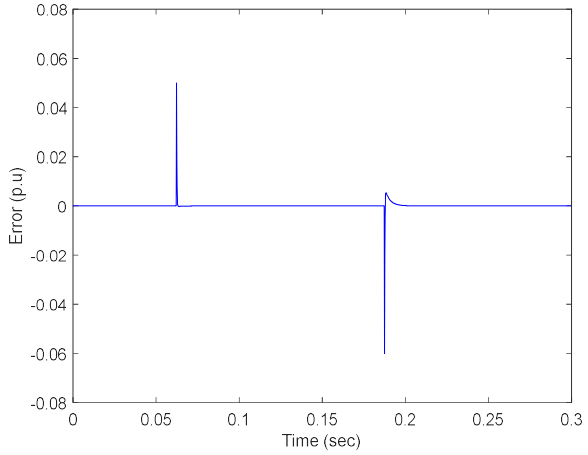

(b) Error of AUKF

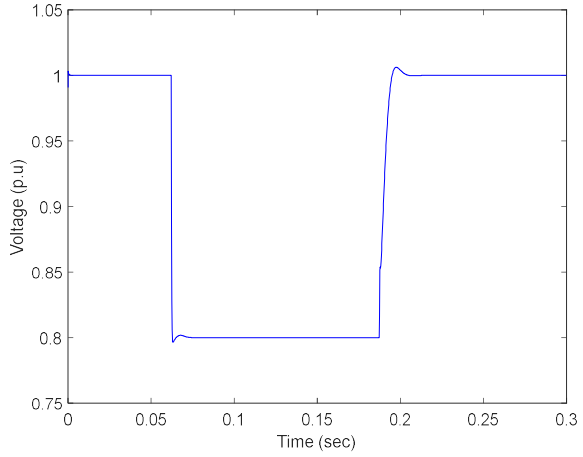

(c) Magnitude estimation

Figure 8. Estimation results of voltage sag with residual magnitude of 0.8 p.u.

In Eq. (12), both the Gaussian process noise and measurement noise variances are assumed to be 0.01 for the prediction and correction steps of the AUKF. The prediction steps are performed sequentially according to Eqs. (13)–(16) to find the values $\hat{\mathbf{X}}_k$ in (16). Then the correction process is performed sequentially according to Eqs. (25)–(30) to determine the adjusting value of the state variables. $\mathbf{X}_k$. The state variable $\mathbf{X}_k$ is a vector containing the state variables of the applied signal that have been modelled as in Eq. (32) including: magnitude U_m and phase angle φ. The error between the estimated and measured voltage sag signals is illustrated in Figure 6b (0.2 p.u.), Figure 7b (0.5 p.u.), and Figure 8b (0.8 p.u.). These results clearly indicate the start and end instants of each sag event, allowing the duration to be determined with high accuracy. In addition, the results of estimating the magnitude of voltage wave are shown in Figure 6c (For voltage sag with the magnitude of 0.2 p.u), Figure 7c (For voltage sag with the magnitude of 0.5 p.u) and Figure 8c (For voltage sag with the magnitude of 0.8 p.u).

V. DISCUSSION

Table 1 presents the quantitative performance of the proposed Augmented Unscented Kalman Filter (AUKF) under three different voltage sag levels with residual magnitudes of 0.2, 0.5, and 0.8 p.u. The results demonstrate that the AUKF consistently achieves low root-mean-square error (RMSE), high detection accuracy, and small duration estimation errors across all cases. Specifically, the RMSE values range from 0.012 p.u. at the deepest sag (0.2 p.u.) to 0.018 p.u. at the mildest sag (0.8 p.u.), indicating that the estimation error remains within a narrow band regardless of sag severity. Moreover, detection accuracy improves slightly as the residual magnitude increases, from 96.5% at 0.2 p.u. to 98.1% at 0.8 p.u., suggesting that the algorithm is more reliable in identifying less severe sags. Importantly, the duration error remains below 2.2 ms in all scenarios, confirming the robustness of the proposed method in capturing the temporal characteristics of voltage sags. Overall, the results in Table 1 validate the effectiveness of the AUKF-based approach, as it maintains both precision and robustness under varying sag conditions, thereby demonstrating suitability for real-time power quality monitoring.

Table 1. Quantitative performance of AUKF under different voltage sag levels.

Residual magnitude (p.u.)	RMSE (p.u.)	Detection accuracy (%)	Duration error (ms)
0.2	0.012	96.5	2.1
0.5	0.015	97.8	1.8
0.8	0.018	98.1	1.6

The numerical results presented in Table 2 demonstrate the advantages of the proposed AUKF-based approach over conventional EKF and UKF techniques. First, in terms of accuracy, AUKF consistently yields the lowest RMSE values across all simulated sag levels achieving reductions of approximately 2.6% compared with EKF and 1.1% compared

with UKF. This improvement can be attributed to the augmented state representation, which captures both fundamental and harmonic components without relying on Jacobian approximations. Second, the detection accuracy of the AUKF consistently exceeds 96.5% across all test cases. In addition, its duration estimation error remains below 3 ms, significantly smaller than those observed with EKF (≈5 ms) and UKF (≈4 ms). These findings confirm the robustness of AUKF for precise temporal characterization of sag events.

Table 2. Comparative Study between EKF, UKF, and AUKF.

Method	RMSE (p.u.)	Detection accuracy (%)	Avg. Duration error (ms)
EKF	0.028	95.2	5.3
UKF	0.021	96.7	3.9
AUKF	0.015	97.8	2.8

VI. CONCLUSIONS

This study introduced an Augmented Unscented Kalman Filter (AUKF)-based framework for voltage sag detection and characterization in power systems. By incorporating augmented state variables to represent both fundamental and harmonic components, the proposed method overcomes the limitations of conventional EKF and UKF approaches, eliminating the need for Jacobian computation and enhancing numerical stability. Simulation results under various sag conditions (0.2, 0.5, and 0.8 p.u.) confirm that the AUKF achieves lower RMSE, higher detection accuracy, and smaller duration estimation errors compared with traditional methods. These findings demonstrate the robustness and precision of the AUKF algorithm, making it suitable for real-time power quality monitoring.

Future work will focus on validating the method with real measurement data and different noise, exploring adaptive strategies for varying harmonic environments, and integrating the AUKF framework with data-driven approaches to further improve event classification and robustness in practical applications.

AUTHOR CONTRIBUTIONS

D. D. Tung: Conceptualization, Methodology, Validation, Writing – original draft, Writing – review & editing. **N. M. Khoa:** Software, Data curation, Visualization, Writing – review & editing. **N. M. Khoa:** Formal analysis, Validation, Writing – review & editing. **D. D. Tung:** Supervision, Project administration, Writing – review & editing. **N. M. Khoa:** Writing – original draft, Literature review, Writing – review & editing. **D. D. Tung:** Supervision, Writing – review & editing.

REFERENCES

Ai, Q., Y. Zhou and W. Xu (2007). Adaline and its application in power quality disturbances detection and frequency tracking. Electric Power Systems Research, **77**(5-6): 462-469.

Bollen, M. H. (2000). Understanding power quality problems, IEEE press New York.

Bollen, M. H. and I. Y. Gu (2006). Signal processing of power quality disturbances, John Wiley & Sons.

Camarillo-Peñaranda, J. R. and G. Ramos (2018). Fault classification and voltage sag parameters computation using voltage ellipses. 2018 IEEE/IAS 54th Industrial and Commercial Power Systems Technical Conference (I&CPS), IEEE.

Costa, F., B. Souza and N. Brito (2010). Real-time detection of voltage sags based on wavelet transform. 2010 IEEE/PES Transmission and Distribution Conference and Exposition: Latin America (T&D-LA), IEEE.

Chang, G. and C.-I. Chen (2010). Performance evaluation of voltage sag detection methods. IEEE PES General Meeting, IEEE.

Choudhury, A. R., R. K. Mallick, R. Agrawal and P. Nayak (2024). Power Quality Disturbance Monitoring in PV Integrated Power System with Mode Decomposition and Ensemble Extreme Learning Machine. Nigerian Journal of Technological Development, **21**(3): 127-135.

Gencer, Ö., S. Öztürk, and T. Erfidan (2010). A new approach to voltage sag detection based on wavelet transform. International Journal of Electrical Power, **32**(2): 133-140.

Granados-Lieberman, D., R. Romero-Troncoso, R. Osornio-Rios, A. Garcia-Perez and E. Cabal-Yepez (2011). Techniques and methodologies for power quality analysis and disturbances classification in power systems: a review. IET Generation, Transmission Distribution, **5**(4): 519-529.

Han, Y., Y. Feng, P. Yang, L. Xu, Y. Xu and F. Blaabjerg (2019). Cause, classification of voltage sag, and voltage sag emulators and applications: A comprehensive overview. IEEE Access, **8**: 1922-1934.

Hartikainen, J., A. Solin and S. Särkkä (2011). Optimal filtering with Kalman filters and smoothers. Department of Biomedica Engineering Computational Sciences, Aalto University School of Science, 16th August, 2011 **10**(1.331): 150.

Hasan, S., K. M. Muttaqi and D. Sutanto (2020). Detection and characterization of time-variant nonstationary voltage sag waveforms using segmented Hilbert–Huang transform. IEEE Transactions on Industry Applications, **56**(4): 4563-4574.

Li, H., C. Meng and Y. Zhao (2022). Automatic expansion of voltage signals using empirical mode decomposition for voltage sag detection. IEEE Access, **10**: 80138-80150.

Mansor, M. and N. A. Rahim (2009). Voltage sag detection-A survey. 2009 International Conference for Technical Postgraduates (TECHPOS), IEEE.

Masoum, M., S. Jamali and N. Ghaffarzadeh (2010). Detection and classification of power quality disturbances using discrete wavelet transform and wavelet networks. IET Science, Measurement Technology, **4**(4): 193-205.

Mishra, S., C. Bhende and B. Panigrahi (2007). Detection and classification of power quality disturbances using S-transform and probabilistic neural network. IEEE Transactions on Power Delivery, **23**(1): 280-287.

Perez, E. and J. Barros (2008). An extended Kalman filtering approach for detection and analysis of voltage dips in

power systems. Electric Power Systems Research, **78**(4): 618-625.

Perez, E. and J. Barros (2008). A proposal for on-line detection and classification of voltage events in power systems. IEEE Transactions on Power Delivery, **23**(4): 2132-2138.

Pérez, E. and J. Barros (2006). Voltage event detection and characterization methods: A comparative study. 2006 IEEE/PES Transmission & Distribution Conference and Exposition: Latin America, IEEE.

Stuart, Z. K., Y. El-Laham and M. F. Bugallo (2021). Robust frequency and phase estimation for three-phase power systems using a bank of Kalman filters. IEEE Signal Processing Letters, **28**: 1235-1239.

Tong, Z., J. Zhong, J. Li, J. Wu and Z. J. Li (2023). A power quality disturbances classification method based on multi-modal parallel feature extraction. Scientific Reports, **13**(1): 17655.

Wang, G., H. Zhang, M. Gao, W. Ding, Y. Qian (2025). Identification and classification of power quality disturbances using CNN-transformer. Journal of Electrical Engineering & Technology, **20**(5): 2993-3007.

Wang, Y., H.-S. He, X.-Y. Xiao, S.-Y. Li, Y.-Z. Chen and H.-X. Ma (2022). Multi-stage voltage sag state estimation using event-deduction model corresponding to EF, EG, and EP. IEEE Transactions on Power Delivery, **38**(2): 797-811.

Yu, Y., W. Zhao, S. Li and S. Huang (2021). A two-stage wavelet decomposition method for instantaneous power quality indices estimation considering inter-harmonics and transient disturbances. IEEE Transactions on Instrumentation Measurement, **70**: 1-13.